



Horizon 2020

H2020-EO-2014 NEW IDEAS FOR EARTH-RELEVANT SPACE APPLICATIONS

EUSTACE

(GRANT AGREEMENT 640171)



EU SURFACE TEMPERATURE FOR ALL CORNERS OF EARTH

DELIVERABLE D3.1

Validation Report for Surface Temperature Uncertainties

Deliverable Title	Validation report for surface temperature uncertainties	
Brief Description	<i>This report details the validation of the uncertainties added to the satellite datasets in CEMS. The report aims to present the outcome of the validation of the satellite uncertainty budgets for land, sea and ice surface temperatures.</i>	
WP number	3	
Lead Beneficiary	<i>Darren Ghent, University of Leicester</i>	
Contributors	<i>Patricio Ortiz, University of Leicester Rasmus Tonboe, DMI Gary Corlett, University of Leicester</i>	
Creation Date	22/01/2016	
Version Number	1.1	
Version Date	09/03/2016	
Deliverable Due Date	31/12/2015	
Actual Delivery Date	09/03/2016	
Nature of the Deliverable	R	<i>R – Report</i>
		<i>DEM – Demonstrator, Pilot, Prototype</i>
		<i>DEC – Dissemination, Exploitation or Communication</i>
		<i>O – Other</i>
Dissemination Level/ Audience	PU	<i>PU – Public</i>
		<i>CO - Confidential, only for members of the consortium, including the Commission services</i>

Version	Date	Modified by	Comments
1	25/01/2016	Darren Ghent	First Draft
1.1	23/02/2016	Darren Ghent	Consistent approach across all domains
1.2	09/03/2016	Darren Ghent	Final Version



Table of Contents

1. Executive Summary	3
2. Data lists	3
3. Unified approach to surface temperature uncertainty validation.....	4
4. Validation results and analysis	5
4.1 Land Surface Temperature	5
4.2 Ice Surface Temperature	11
4.3 Sea Surface Temperature	14
4. Summary.....	19
5. References	20
6. Appendix A – Simulated Ice Surface Temperature Uncertainties.....	21

1. Executive Summary

This report presents the outcome of validating the uncertainties included with the satellite-derived surface temperature data sets within the EUSTACE project, i.e., the total uncertainties for each satellite skin pixel / grid-cell observation of the oceans, land, and ice surfaces. Each satellite-derived data type includes three components of uncertainty representing the uncertainty from effects whose errors have distinct correlations properties: random, locally systematic, and systematic. Here, we validate the total of these uncertainty components.

2. Data lists

A detailed list of all the satellite uncertainty data estimated by EUSTACE is provided in D1.3 (Uncertainties added to satellite datasets in CEMS). Here, we briefly summarise the data types for which we assess those uncertainty estimates in this report:

- Satellite sea surface temperatures from ESA SST CCI (A)ATSR L3U Long-term product
- Land surface skin temperature data sets from GlobTemperature:
 - Satellite LST data derived from Aqua-MODIS (GT_MYG_2P)
 - Satellite LST data derived from SEVIRI (GT_SEG_2P)



- Ice surface skin temperature observations (sea ice and ice sheets) from AVHRR GAC reanalysis:
 - Arctic and Antarctic ice Surface Temperatures from thermal Infrared satellite sensors (AASTI)

Note: Since input SEVIRI LST data has not been processed to date for a sufficiently long time period for meaningful statistics to be extracted, no validation of these uncertainties has been carried out in the framework of this report.

3. Unified approach to surface temperature uncertainty validation

The approach to validating the estimated uncertainties of the surface temperature (ST) satellite products is to compare the standard deviation of the differences between the satellite-derived ST and in situ measurements with the total uncertainties of such validation pairs (matchups). In other words, we test the goodness-of-fit between the difference from in situ reference data ($\sigma_{sat-ground}$) and the total uncertainty for each associated matchup (σ_{total}), where σ_{total} is determined from four components:

$$\sigma_{total} = \sqrt{\sigma_{sat}^2 + \sigma_{ground}^2 + \sigma_{space}^2 + \sigma_{time}^2}$$

For each matchup σ_{sat} is the total ST uncertainty for each satellite pixel as derived for each product; σ_{ground} is the uncertainty associated with the ground-based instrumentation; σ_{space} is the uncertainty associated with matching a satellite and ground observation in a spatial context; and σ_{time} is the uncertainty associated with matching a satellite and ground observation in time. Note that the uncertainty estimates were created by modelling different components of the retrievals and without reference to in situ data, so our results represent a completely independent validation of this information.

The general approach is consistent for all of LST, IST and SST. For LST and IST these validations are carried out for each in situ validation site independently since the components - σ_{ground} , σ_{space} and σ_{time} - are site-dependent. For SST, we compare the robust standard deviation (RSD) of the discrepancy between the satellite SST and drifting buoy network as a function of the measurement uncertainty according to the multi-sensor match-up system (MMS) (Corlett et al., 2014), whereby drifting buoy and satellite



observations are matched globally under clear-sky conditions. There is a lower limit on this model of ± 0.15 K which represents the uncertainty in the drifting buoy measurements (σ_{ground}). In addition to the other the terms σ_{space} and σ_{time} , for SST there is also the difference in depth of the measurements to consider (σ_{depth}).

4. Validation results and analysis

4.1 Land Surface Temperature

In order to validate the uncertainty data accompanying the Aqua-MODIS Level-2 LST product (GT_MYG_2P), in-situ observations from seven stations of the SURFRAD network (Table 1) over two separate years (2008 and 2011) have been used. This network has become well established as an important source of ground-based measurements for the LST validation community based on its uniformity of methodology and instrumentation. LST values are derived from incoming and outgoing IR radiance measurements made by facing upward and downward pyrgeometers (Eppley Precision Infrared Radiometers).

Table 1. SURFRAD stations used in the validation of the uncertainty budget for the Aqua-MODIS LST product (GT_MYG_2P)

Station Code	Location	Latitude	Longitude	Elevation (m)
BON	Bondville, Illinois	40.05	-88.37	213
DRA	Desert Rock, Nevada	36.62	-116.02	1007
FPK	Fort Peck, Montana	48.30	-105.10	634
GWN	Goodwin Creek, Mississippi	34.25	-89.87	98
PSU	Penn State University PA	40.72	-77.93	376
SXF	Sioux Falls, South Dakota	43.73	-96.62	473
TBL	Table mountain, Colorado	40.12	-105.24	1689

The matchup procedure can be briefly summarized as follows:

- The spatial matching is done by first determining the satellite pixel that is closest in space to the location of the in situ station. The satellite pixels have a nominal resolution at nadir of 1 km, and 5 x 5 pixels around the closest pixel are merged into one matchup grid for comparison.
- The data from these pixels is averaged taking the median of the LST of the single pixels. Only grid points where at least 20 pixels are not flagged as being cloud contaminated are considered, since in areas where a larger fraction is cloud flagged the possibility of not masked cloud edges is increased.
- The in situ observation from the nearest minute (see below) is used in the matchup process to minimize unrepresentative matchups in time.

All SURFRAD sites report in situ measurements at a temporal rate of 60 seconds, the measurements themselves being the mean over the preceding 60 seconds. With such a high rate of measurement the uncertainty associated with matching a satellite and ground observation in time (σ_{time}) can be assumed to have a negligible contribution to the total uncertainty for each matchup (σ_{total}). The uncertainty associated with matching a satellite and ground observation in a spatial context (σ_{space}) has been estimated for each site as the standard deviation of all clear-sky surface temperatures of the highest quality in the 5 x 5 matchup grid for each individual matchup.

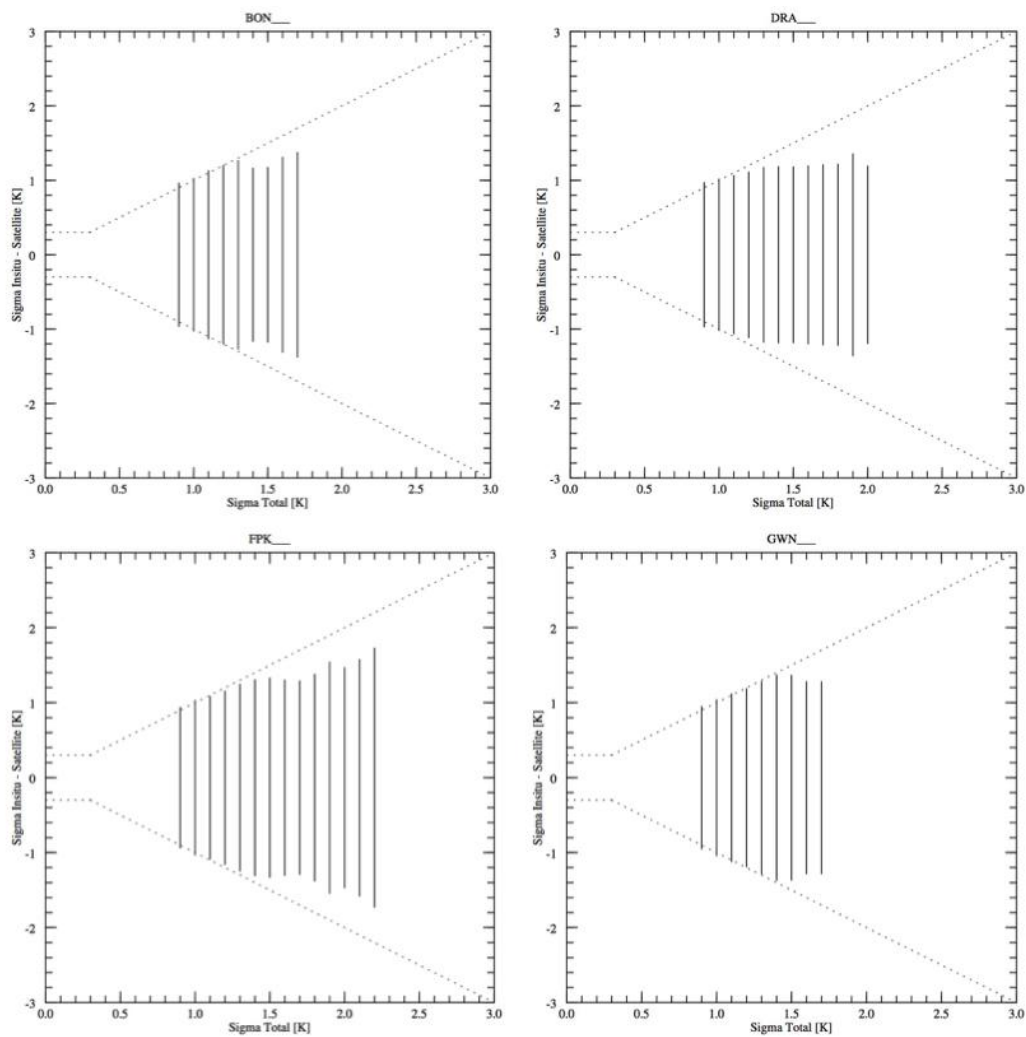
The uncertainty associated with the ground-based instrumentation (σ_{ground}) is a propagation of the nominal uncertainty associated with (i) measuring the radiance with the upwelling and downwelling pyrgeometers which theoretically should be the same for each station, since each SURFRAD site has been installed with the same instrumentation which is regularly recalibrated on the same temporal frequency, and (ii) estimating the broadband emissivity (BBE) at each site. The uncertainty of the BBE is composed of the uncertainties of the input IR global land surface emissivities (Seemann et al., 2008) and the uncertainty of the fitting equation. For the former, Borbas and Ruston (2010) give a standard deviation between 0.005 and 0.02 for the single wavelengths, and for the latter Cheng et al. (2013) specify a RMSE of 0.005. Using uncertainty propagation of these input emissivity uncertainties and the input fitting uncertainty an upper value of 0.01 is estimated. For the measured radiances from field pyrgeometers the uncertainty is estimated to be $\pm 5 \text{ Wm}^{-2}$ (Augustine and Dutton, 2013).

Figure 1 illustrates the comparison between σ_{total} and $\sigma_{sat-ground}$ for each of the SURFRAD stations during a full year of observations (2011). The comparison is carried out for each 0.1 K bin of σ_{total} . The curves in Figure 1 (and subsequent Figures) are theoretical and represent the idealised case of a representative site with well characterised satellite uncertainty. If the uncertainty model is correct then $\sigma_{sat-ground}$ estimates should fit within and intersect with the 1:1 dashed lines for each σ_{total} 0.1 K bin. In general the fit appears to be relatively good for most sites particularly for lower uncertainty bins, and remaining relatively stable across the bins of σ_{total} . Even so, larger differences become more evident between $\sigma_{sat-ground}$ and σ_{total} at higher bins. These differences reveal that σ_{total} is being overestimated for larger values. The consistent in situ instrumentation suggest σ_{ground} is unlikely to be the primary cause of this overestimate. Furthermore, the most homogeneous of sites (SXF) shows good agreement across the bins. This suggests that the satellite uncertainty estimates (σ_{sat}) capture the uncertainty in the LST well for this site. The implication is that the primary cause of the overestimate at higher bins of σ_{total} is an overestimate in σ_{space} . This could be a result of cloud contamination in the 5 x 5 matchup grid or an unrepresentative scaling from the in situ point to the matchup area. In other words the standard deviation of the 5 x 5 region of interest may not accurately represent the difference between the in situ measurement and the mean of the 5 x 5 satellite pixels if the station is measuring an unrepresentative surface in the context of the wider landscape, often described as the point-to-area problem.

The analysis is also repeated for an alternative year (2008) to check for consistency of the validation results. The fit for each site (Figure 2) is found to be consistent between the two years of analysis, whereby the most homogeneous of sites (SXF) produces the best fit. It is also notable that in both cases the PSU site shows the least optimum fit while concurrently producing the widest range of σ_{total} . This site is the most heterogeneous with urban pixel contamination within the matchup making it challenging to resolve the point-to-area problem. While the evidence from both years of analysis suggests that the difference in surface characterisation between the in situ field of view and the mean of the 5 x 5 satellite pixels is primarily responsible for the overestimation in σ_{total} , the persistence of undetected cloud should also not be discounted. The most unrepresentative sites (PSU and DRA in particular) include strong LST gradients across the matchup grid. This explains the plateau effect for these sites since the spatial component (σ_{space}) considers an area which is composed of more extreme values increasing the standard deviation. This is not represented in the y-axis

though which considers the difference between the in situ and the mean of the area; the mean being relatively well constrained compared with the standard deviation.

Nevertheless, the good agreement for the more homogeneous SXF site, the good agreement for the other sites at low uncertainty values, and the consistent behaviour at all sites indicate that the satellite uncertainty model for LST is correctly capturing the main sources of uncertainty in the satellite observations.



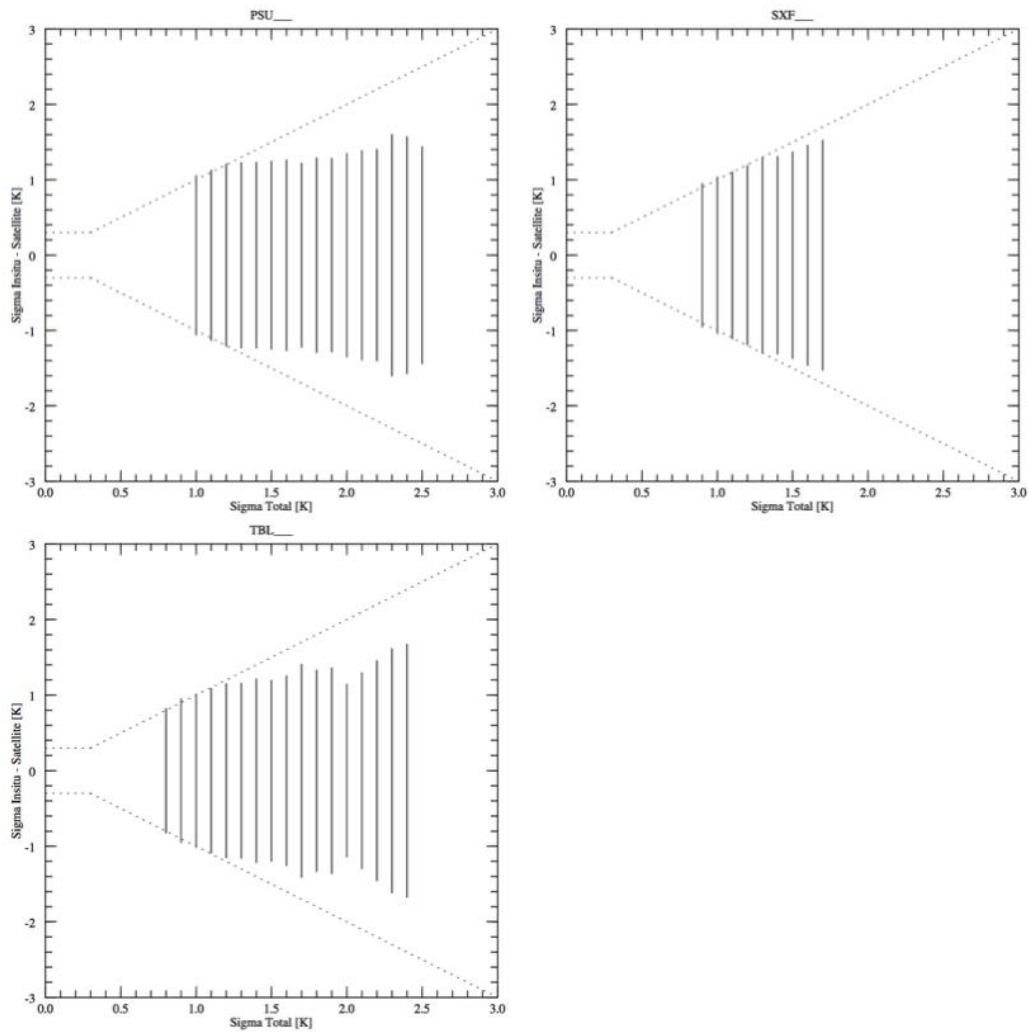
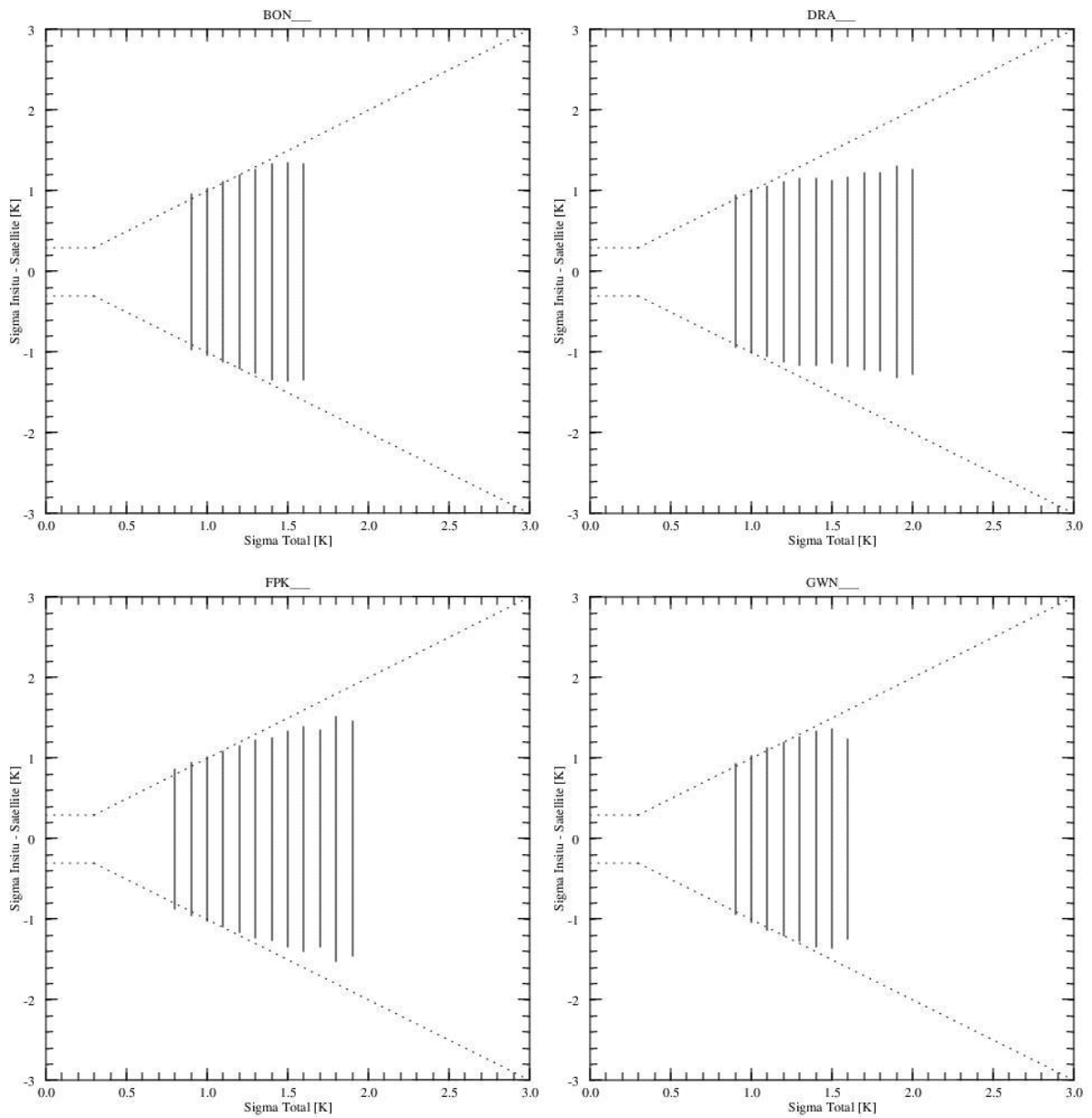


Figure 1. Aqua-MODIS LST uncertainty validation with respect to SURFRAD in-situ data for 2011. Dashed lines show ideal uncertainty model accounting for uncertainties in the in situ data and geophysical uncertainties arising from spatial and temporal collocation. Solid black lines show one standard deviation of the retrieved minus in situ LST differences for each 0.1 K bin.



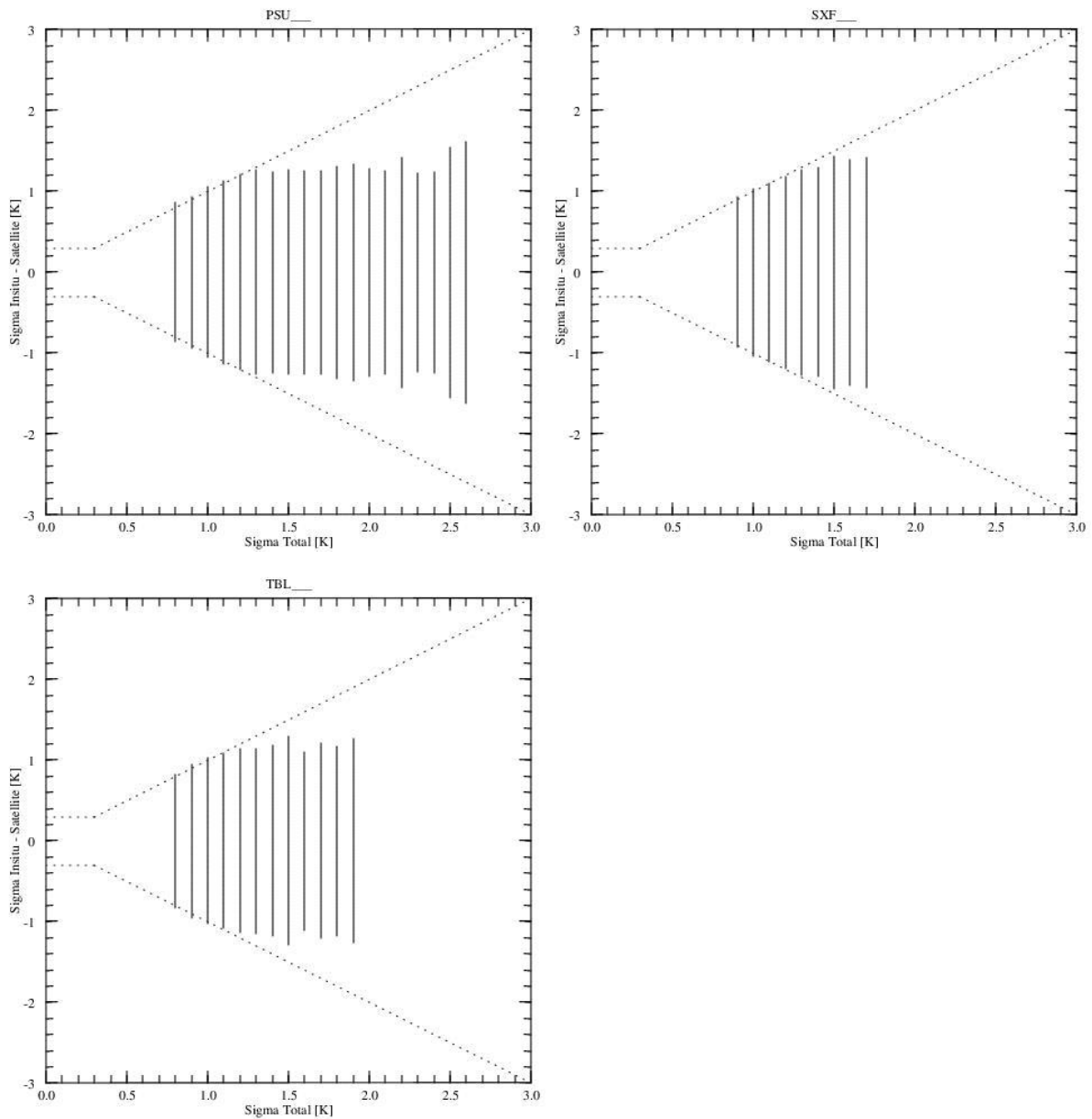


Figure 2. Aqua-MODIS LST uncertainty validation with respect to SURFRAD in-situ data for 2008. Dashed lines show ideal uncertainty model accounting for uncertainties in the in situ data and geophysical uncertainties arising from spatial and temporal collocation. Solid black lines show one standard deviation of the retrieved minus in situ LST differences for each 0.1 K bin.

4.2 Ice Surface Temperature

In order to validate the uncertainty data accompanying the Arctic and Antarctic ice Surface Temperatures from thermal Infrared satellite sensors (AASTI) Level-2 IST product, in-situ observations from two stations of the Atmospheric Radiation Measurement (ARM) network (Table 2) over two years (2008 and 2009) have been used. These are the only two stations



measuring radiometric temperature over several years in the Arctic. This network is well established as an important source of ground-based measurements for both LST and IST validation with uniformity of methodology and instrumentation.

Table 2. ARM stations used in the validation of the uncertainty budget for the AATSI IST product

Station Code	Location	Longitude	Longitude	Elevation (m)
NSA_C1	Barrow, North Slopes of Alaska	71.32	-156.61	8
NSA_C2	Atqasuk, North Slopes of Alaska	70.47	-157.41	20

For NSA_C1 IST values are derived from brightness temperatures measured using a Heitronics KT19.85 Infrared Thermometer. For NSA_C2 IST values are derived from incoming and outgoing IR radiance measurements made by facing upward and downward pyrgeometers (Eppley Precision Infrared Radiometers). The matchup procedure follows the same steps as defined for LST (Section 4.1).

Both ARM sites report in situ measurements at a temporal rate of 60 seconds, the measurements themselves being the mean over the preceding 60 seconds. As for the LST case, with such a high rate of measurement the uncertainty associated with matching a satellite and ground observation in time (σ_{time}) can be assumed to have a negligible contribution to the total uncertainty for each matchup (σ_{total}). The uncertainty associated with matching a satellite and ground observation in a spatial context (σ_{space}) has been estimated for each site as the standard deviation of all clear-sky surface temperatures of the highest quality in the 5 x 5 matchup grid for each individual matchup.

The uncertainty associated with the ground-based instrumentation (σ_{ground}) is a propagation of the nominal uncertainty associated with (i) measuring the brightness temperature with the infrared thermometer for NSA_C1 or measuring the radiance with the upwelling and downwelling pyrgeometers for NSA_C2, and (ii) estimating the broadband emissivity (BBE) at each site. For the measured brightness temperatures from the infrared thermometers the uncertainty is estimated to be ± 0.2 K (Morris, 2006). For the measured radiances from field pyrgeometers the uncertainty is estimated to be ± 5 Wm⁻² (Augustine and Dutton, 2013). The uncertainty of the BBE is defined in the same way as for LST (Section 4.1).

Figures 3 and 4 illustrate the comparison between σ_{total} and $\sigma_{sat-ground}$ for both ARM stations during 2008 and 2009 respectively. The comparison is carried out for each 0.1 K bin of σ_{total} . It is clear that for both stations the fit is very good with only small over estimation at high values of σ_{total} . Unlike over non-snow covered land (as in Section 4.1) the spatial component here is well characterised because the surface is relatively homogeneous with near constant emissivity. The result is that the point-to-area component (σ_{space}) is minimised and we can be confident the matchups are comparing near-equivalent properties. Any residual difference in the fit may be a result of undetected cloud, since cloud clearing over snow / ice surfaces is a particular challenge; this appears at the higher values of σ_{total} . Overall the evidence indicates that the satellite uncertainty model for IST is correctly capturing the main sources of uncertainty in the satellite observations. Complementary to this consistent approach to uncertainty validation, the simulated total IST uncertainty using the forward uncertainty model was assessed against the histogram of the satellite temperatures minus and the infrared radiometer temperatures (see Appendix A).

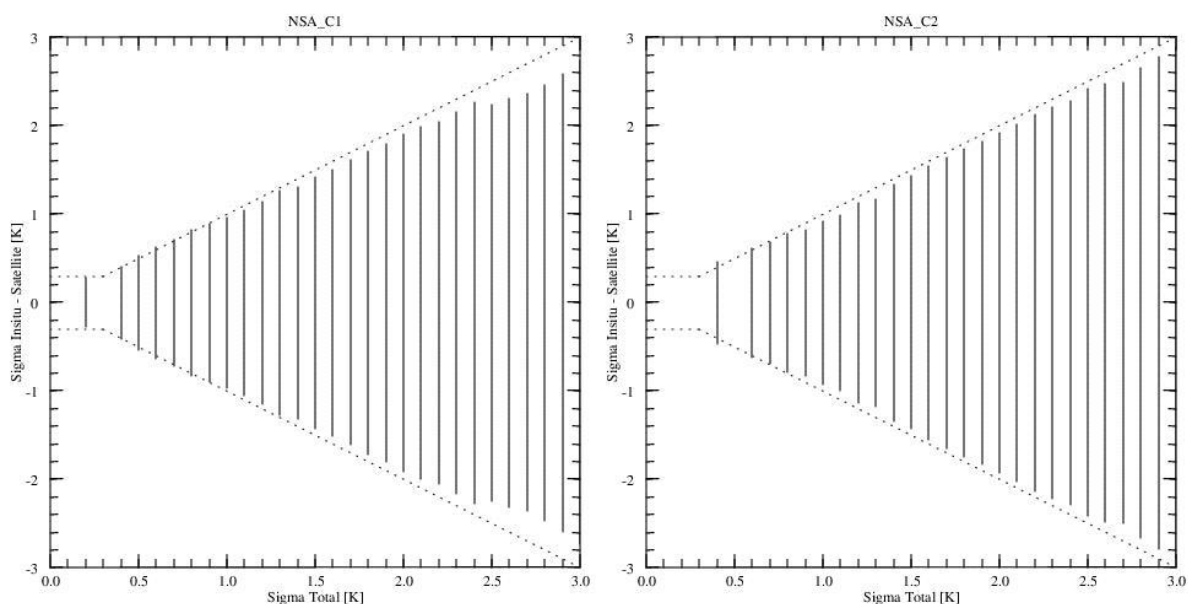


Figure 3. AASTI IST uncertainty validation with respect to ARM in-situ data for 2008. Dashed lines show ideal uncertainty model accounting for uncertainties in the in situ data and geophysical uncertainties arising from spatial and temporal collocation. Solid black lines show one standard deviation of the retrieved minus in situ IST differences for each 0.1 K bin.

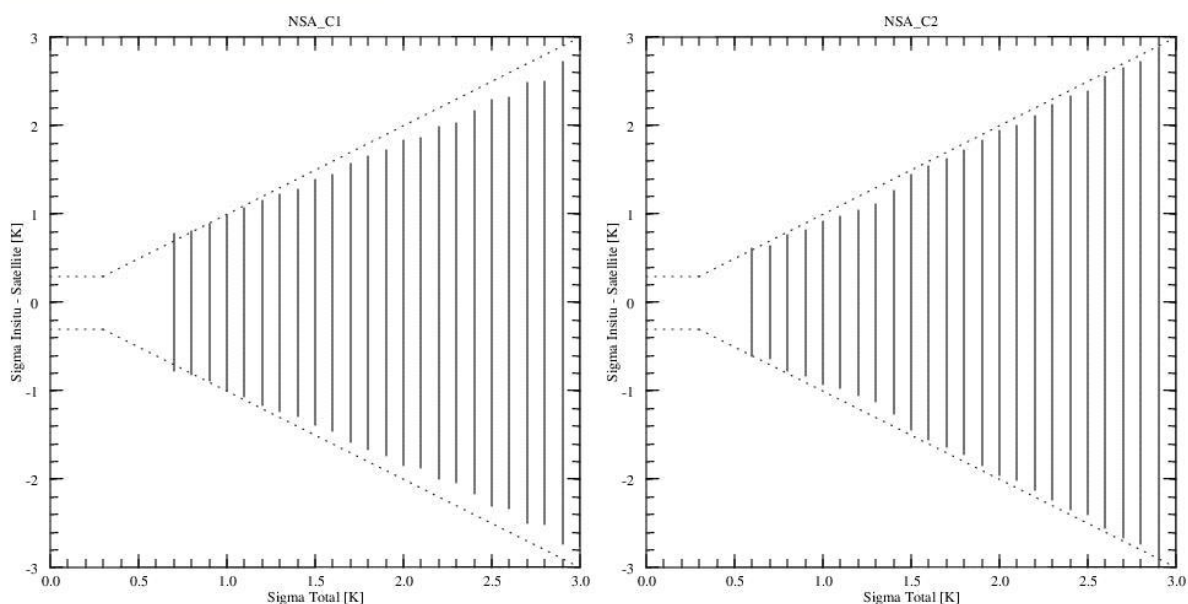


Figure 4. AASTI IST uncertainty validation with respect to ARM in-situ data for 2009. Dashed lines show ideal uncertainty model accounting for uncertainties in the in situ data and geophysical uncertainties arising from spatial and temporal collocation. Solid black lines show one standard deviation of the retrieved minus in situ IST differences for each 0.1 K bin.

4.3 Sea Surface Temperature

The EUSTACE SST data are a “bespoke” run of the processor used in the ESA Climate Change Initiative project on SST, directly outputting at the required resolution of 0.25 deg. Here we present the results of the validation of the uncertainty budget specifically for this bespoke run according to the approach above (as detailed in Section 3) which is consistent with that from SST_CCI (Corlett et al., 2014).

At low satellite uncertainties the standard deviation of the differences is dominated by the uncertainty in the reference data. As you move to higher satellite uncertainties the satellite uncertainty will then dominate as the reference uncertainty becomes a less significant contribution to the total uncertainty. The unified approach outlined in Section 3 considers uncertainty due to environmental effects related to the homogeneity of a region/process. For example, validation in a region dominated by fronts at low wind speed (σ_{space}) will be systematic for any one single match-up. However, as the number of match-ups increases the uncertainty will reduce by $1 / \sqrt{N}$ as you sample the variability at multiple locations. Consequently, the effect is considered to be a pseudo-random term and not a systematic term. Likewise, in an area of strong solar radiation and low wind speed the difference in depth (σ_{depth}) would be systematic for any one match-up.

We attempt to reduce the three terms - σ_{space} , σ_{time} and σ_{depth} - to $\ll 0.1$ K in the mean through the use of a depth/time adjustment, large number of match-ups (to reduce pseudo-random terms) and through like versus like (SST_{skin} versus SST_{skin} or SST_{depth} versus SST_{depth}) comparisons. For that reason, these terms are neglected in the uncertainty validation.

The uncertainty validation results for the EUSTACE SST product are illustrated in Figures 5 (daytime) and 6 (night-time) for AATSR, Figures 7 (daytime) and 8 (night-time) for ATSR-2, and Figures 9 (daytime), 10 and 11 (night-time 2 and 3 channel respectively) for ATSR-1. These show a very good agreement particularly at night-time for the 3-channel SST. It is notable that for ATSR-1 the fit for 3-channel night-time is much improved upon the 2-channel night-time. For daytime the fits are still good particularly at the lower end of σ_{total} , but for higher values the uncertainties appear to be under-estimated from AATSR and ATSR-1 and over-estimated for ATSR-2. It should be noted though that the magnitude of σ_{total} , for SST is approximately a factor of 10 lower than for LST and IST. These results are comparable with those in Corlett et al., 2014 which report the standard error to be fairly consistent across all uncertainties. In conclusion the evidence indicates that the satellite uncertainty model for SST is correctly capturing the main sources of uncertainty in the satellite observations.

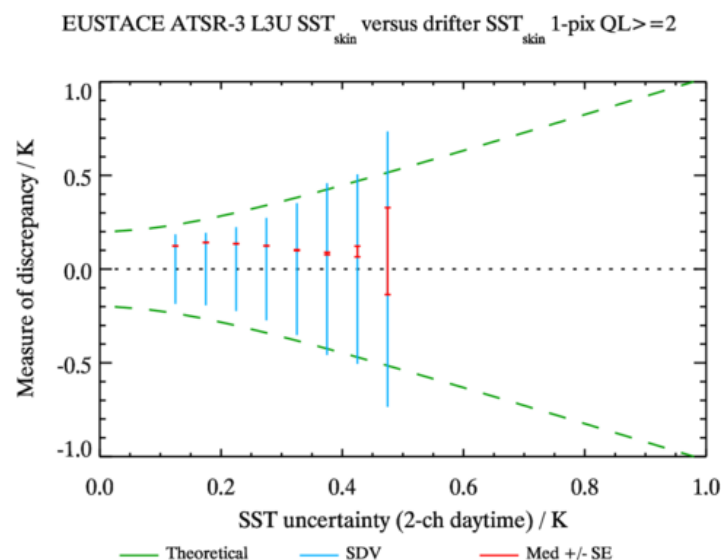


Figure 5. Uncertainty validation of daytime EUSTACE AATSR 2-channel SST_{skin} retrievals assessed against drifter SST_{skin} . Results are shown for pixels with a quality level > 2 . An additional adjustment has been made using a combined diurnal variability/skin model to account for the difference in depth and time between the satellite and drifter measurements.

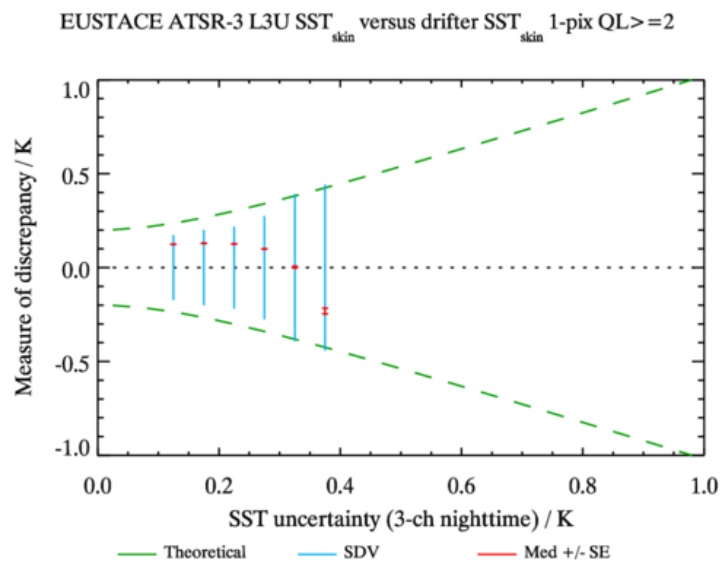


Figure 6. Uncertainty validation of night-time EUSTACE AATSR 3-channel SST_{skin} retrievals assessed against drifter SST_{skin}. Results are shown for pixels with a quality level > 2. An additional adjustment has been made using a combined diurnal variability/skin model to account for the difference in depth and time between the satellite and drifter measurements.

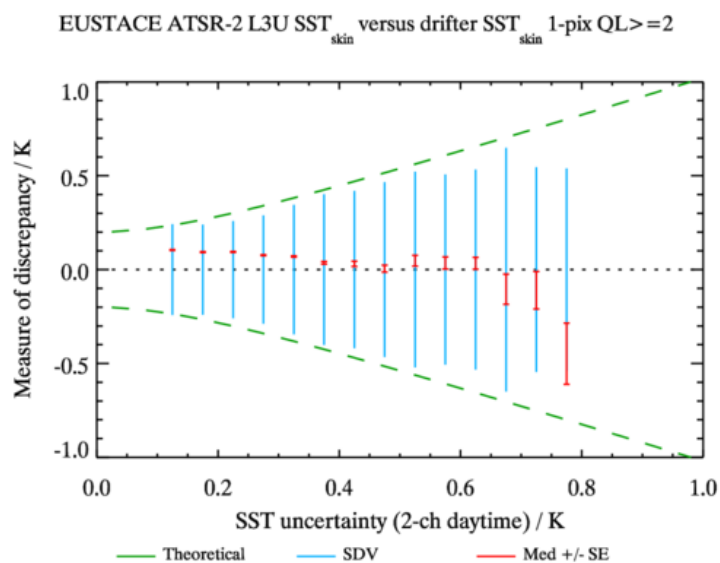


Figure 7. Uncertainty validation of daytime EUSTACE ATSR-2 2-channel SST_{skin} retrievals assessed against drifter SST_{skin} . Results are shown for pixels with a quality level > 2 . An additional adjustment has been made using a combined diurnal variability/skin model to account for the difference in depth and time between the satellite and drifter measurements.

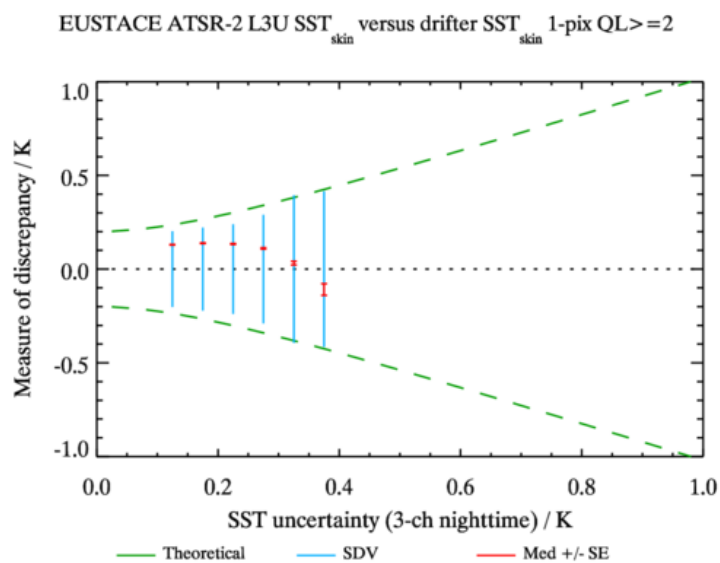


Figure 8. Uncertainty validation of night-time EUSTACE ATSR-2 3-channel SST_{skin} retrievals assessed against drifter SST_{skin} . Results are shown for pixels with a quality level > 2 . An additional adjustment has been made using a combined diurnal variability/skin model to account for the difference in depth and time between the satellite and drifter measurements.

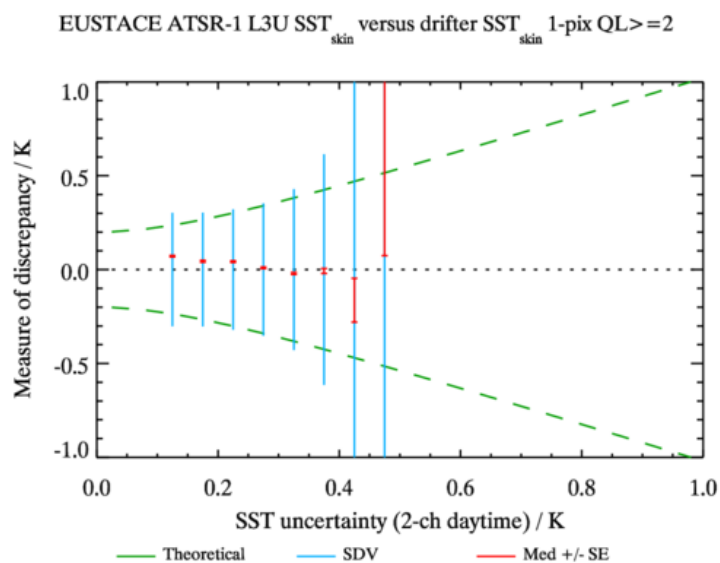


Figure 9. Uncertainty validation of daytime EUSTACE ATSR-1 2-channel SST_{skin} retrievals assessed against drifter SST_{skin} . Results are shown for pixels with a quality level > 2 . An additional adjustment has been made using a combined diurnal variability/skin model to account for the difference in depth and time between the satellite and drifter measurements.

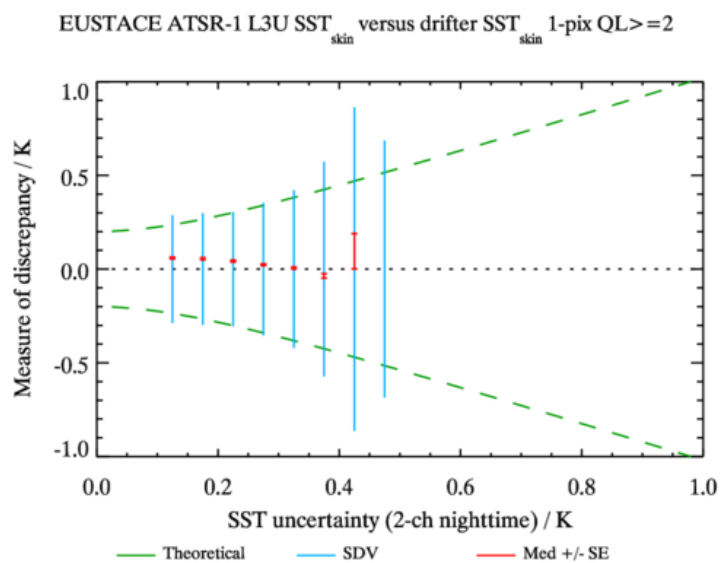


Figure 10. Uncertainty validation of night-time EUSTACE ATSR-1 2-channel SST_{skin} retrievals assessed against drifter SST_{skin} . Results are shown for pixels with a quality level > 2 . An additional adjustment has been made using a combined diurnal variability/skin model to account for the difference in depth and time between the satellite and drifter measurements.

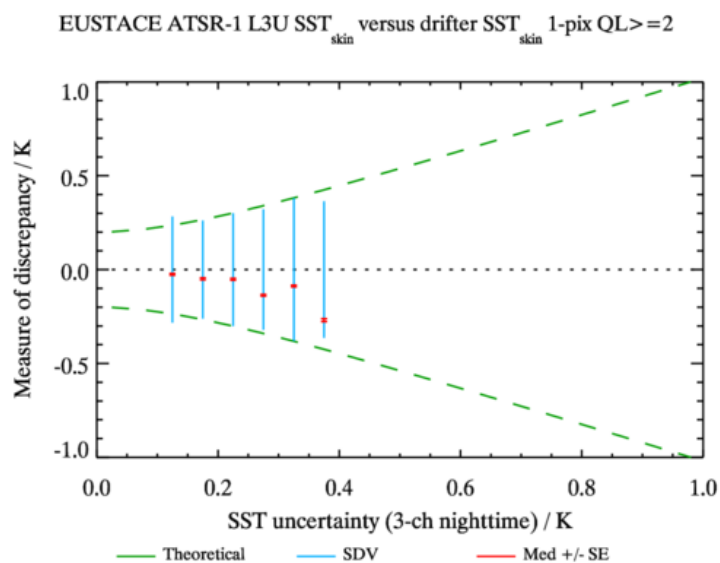


Figure 11. Uncertainty validation of night-time EUSTACE ATSR-1 3-channel SST_{skin} retrievals assessed against drifter SST_{skin}. Results are shown for pixels with a quality level > 2. An additional adjustment has been made using a combined diurnal variability/skin model to account for the difference in depth and time between the satellite and drifter measurements.

4. Summary

This report presents the validation results for the uncertainty information included with the satellite-derived surface temperature data sets for sea, land and ice within the EUSTACE project. It demonstrates that we can have confidence in the consistency of the uncertainties we have estimated between ocean, land and ice. Information on the methods used to derive the uncertainties and the end-products are detailed in D1.2 and D1.3. For LST the good agreement at a homogeneous site coupled with the good agreement for the other sites at low uncertainty values, and the consistent behaviour at all sites indicate that the satellite uncertainty model for LST is correctly capturing the main sources of uncertainty in the satellite observations. For IST the validation is carried out over two stations where the impact of spatial matching is minimized as a result of the homogeneous surface. The results show that the satellite uncertainty model is accurately capturing the uncertainty in the satellite observations. For SST there is also generally a very good agreement particularly at night-time for all three sensors of the ATSR series. For daytime also the agreement is good for lower uncertainty estimates and overall the uncertainty model can be concluded as deriving a good representation of the uncertainty in the satellite observations.



The improved estimation of uncertainties for Ice Surface Temperature in EUSTACE is now being transferred to the operational processing of IST in EUMETSAT's OSISAF so that the operational users will have access to these. The same is happening for the gridded (L4) products in the Copernicus marine service.

5. References

Augustine, J. A., and E. G. Dutton, *Variability of the surface radiation budget over the United States from 1996 through 2011 from high-quality measurements*. J. Geophys. Res. Atmos., 2013. **118**: p. 43–53.

Borbás, E.E. and B. C. Ruston, *The RTTOV UWiremis IR land surface emissivity module*. Associate Scientist mission report Mission no. AS09-04 Document NWPSAF-MO-VS-042, 2010

Bulgin, C.E., Embury, O., Corlett, G., and Merchant, C.J., *Independent uncertainty estimates for coefficient based sea surface temperature retrieval from the Along-Track Scanning Radiometer instruments*. Remote Sensing of Environment, 2016 (in review),

Cheng, J., S. Liang, Y. Yao, and X. Zhang, *Estimating the optimal broadband emissivity spectral range for calculating surface longwave net radiation*. IEEE Geoscience and Remote Sensing Letters, 2013. **10**: p. 401–405

Corlett et al., 2014, Product Validation and Intercomparison Report (PVIR), SST_CCI-PVIR-UoL-001

D1.2 Common approach to providing uncertainty estimates across all surfaces (September 2015)

D1.3 Uncertainties added to satellite datasets in CEMS (December 2015)

Dozier, J., S. G. Warren. 1982. Effect of viewing angle on the infrared brightness temperatures of snow. Water resources research 18(5), 1424-1434.

Drifter SST_{depth} adjusted to drifter SST_{skin} using combined skin-effect (Fairall et al., 1996) and diurnal variability model (Kantha and Clayson, 1994).

Fairall, C., E. Bradley, J. Godfrey, G. Wick, J. Edson, and G. Young (1996), Cool-skin and warm-layer effects on sea surface temperature, J. Geophys. Res., 101(C1), 1295-1308.

Kantha L.H., and Clayson C.A., An improved mixed layer model for geophysical applications. J. Geophys. Res. Vol. 99 (C12), 25235–25266, 1994.

Morris, V. R., *Infrared Thermometer (IRT) Handbook (ARM TR-015)*. Atmospheric Radiation Measurement, Climate Research Facility, U. S. Department of Energy, 2006. (https://www.arm.gov/publications/tech_reports/handbooks/irt_handbook.pdf)

Seemann, S.W., E. E. Borbas, R. O. Knuteson, G. R. Stephenson, H.-L. Huang, *Development of a global infrared land surface emissivity database for application to clear sky sounding retrievals from multispectral satellite radiance measurements*. Journal of Applied Meteorology and Climatology, 2008. **47**(1): p. 108-123.

6. Appendix A – Simulated Ice Surface Temperature Uncertainties

A supplementary approach to assessing the validity of uncertainties was also carried out in the IST case. Here surface temperatures are validated using in situ thermometer or radiometer measurements. For the uncertainties: the total uncertainty from the forward model is compared to the variability of the satellite - in situ differences and these should match up when neglecting the in situ uncertainties. Validating the individual components in the uncertainty budget requires specialized and controlled experiments. The two figures below demonstrate (1) the comparison between the total uncertainty using our uncertainty forward model and the satellite - in situ variability giving a good match in terms of both bias and STD (Figure 12); and (2) the simulated variability of the snow surface emissivity for the AVHRR channel 3, 4, and 5 using realistic and measured distributions of snow grain size and density and an emissivity model (Figure 13). The variability of the emissivity translates into one of the components in the uncertainty budget and an element in the forward model for uncertainty.

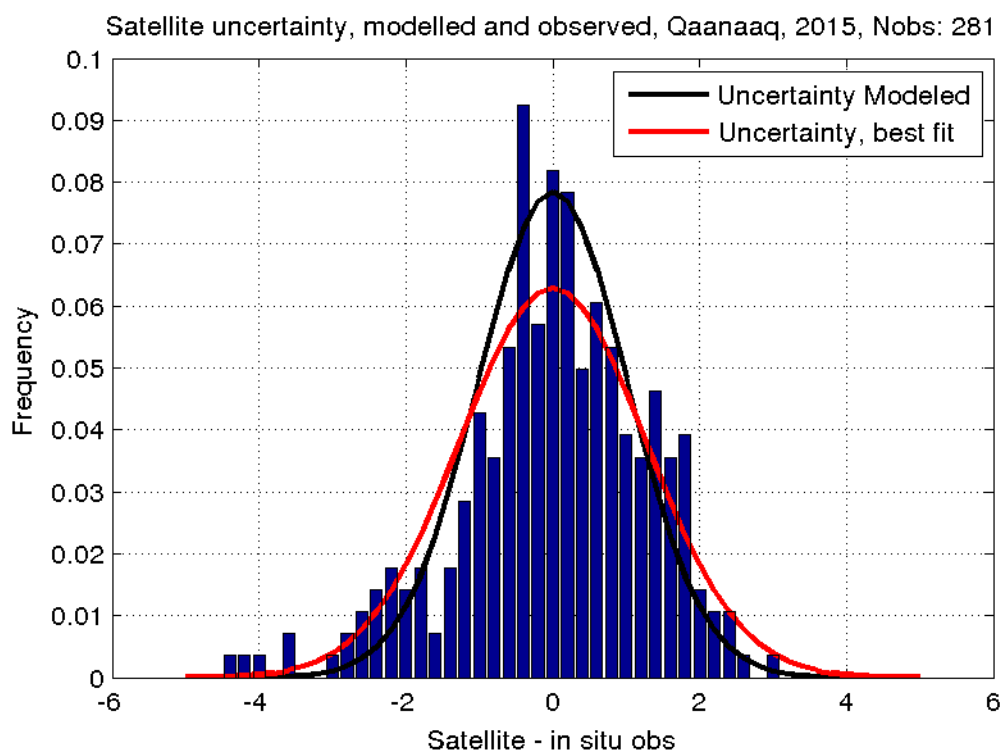


Figure 12. Comparison between the MetOp AVHRR IST (Satellite) and the temperature measured by an infrared radiometer pointed downwards (CS IR120) mounted on a weather station on the sea ice in North West Greenland (77.43N; 69.14W). The frequency of the satellite - in situ differences are shown as blue bars. The red curve is showing the gaussian fit to the blue bars and the black curve is showing the simulated total uncertainty using the forward uncertainty model.

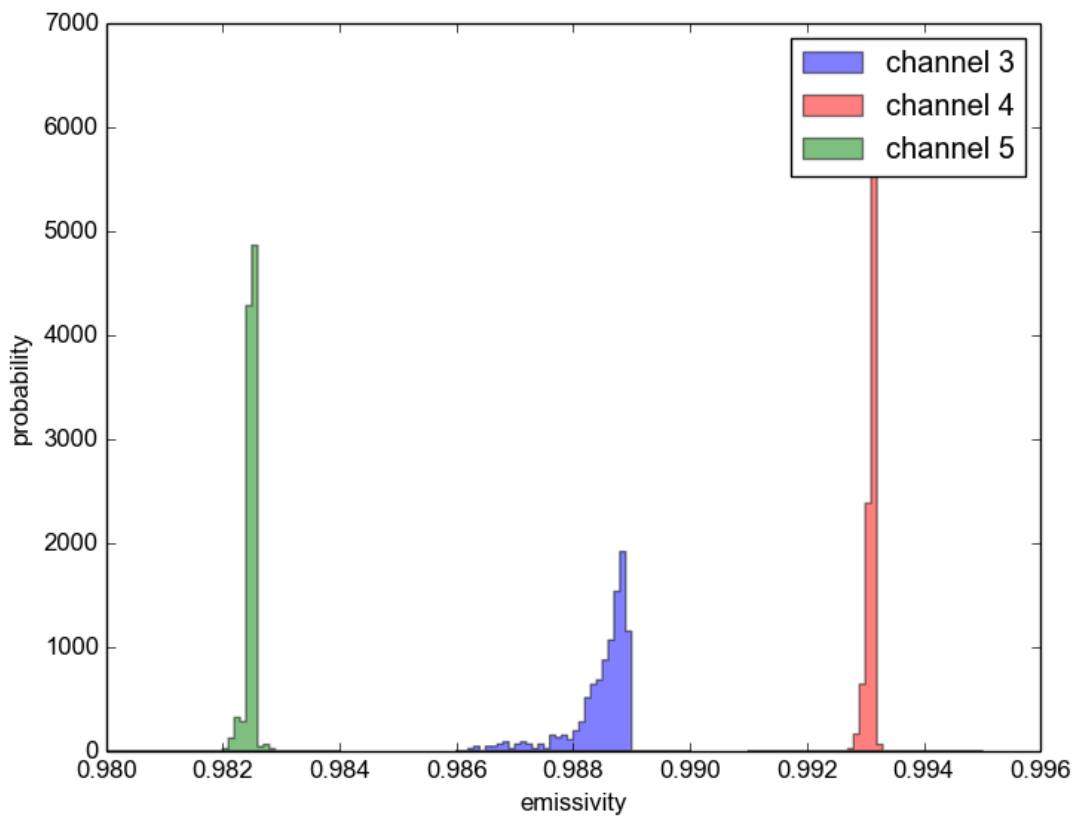


Figure 13. Simulated variability of the snow surface emissivity for the AVHRR channel 3, 4, and 5 using realistic and measured (in situ) distributions of snow grain size and density and an emissivity model (Dozier and Warren, 1982). Channels 4 and 5 are input to the IST retrieval algorithm.